Available online at www.sciencedirect.com
SCIENCE DIRECT®
Journal of Chromatography A, 1049 (2004) 161–169
JOURNAL OF CHROMATOGRAPHY A
www.elsevier.com/locate/chroma

Characterization of Co, Fe and Mn-exchanged zeolites by inverse gas chromatography

Eva Díaz, Salvador Ordóñez*, Aurelio Vega, José Coca

Department of Chemical Engineering and Environmental Technology, University of Oviedo, Julián Clavería s/n, 33006 Oviedo, Spain

Received 19 May 2004; received in revised form 23 July 2004; accepted 27 July 2004

Abstract

The adsorption of several alkanes, cyclic hydrocarbons, aromatic hydrocarbons and chlorinated compounds on NaX, CaA, and exchanged Co, Mn and Fe zeolites as adsorbents was investigated. Zeolite composition and structure was determined by ICP-mass spectroscopy, XRD, and nitrogen adsorption. Adsorption parameters (enthalpy of adsorption and free energy of adsorption) as well as dispersive surface energy interaction and specific interaction parameters were determined for each solute–adsorbent system by inverse gas chromatography (IGC). The original zeolites NaX and CaA show the higher values of enthalpy of adsorption but specific interactions depend on the metal exchanged. Zeolites Mn–NaX and Co–NaX exhibit the strongest interactions with benzene, whereas zeolite Co–CaA shows the strongest interactions with chlorinated compounds. The trivalent cation (Fe^{3+}) does not affect the either the adsorption efficiency or specific interaction.

Keywords: Zeolites; Transition metals

1. Introduction

Zeolites and molecular sieves are porous materials of widespread use as catalysts, sorbents and ion exchangers in petroleum refining and other chemical processes [1]. Zeolites are a group of crystalline aluminosilicates with a cage-like structure of SiO_4 and AlO_4 tetrahedra bound by shared oxygen atoms. The negative charges of the AlO_4 units are balanced by exchangeable cations—Na^+, K^+, Ca^{2+}, Mg^{2+} or Fe^{3+}. These ions can be easily exchanged by other ions and the high exchange capacity of zeolites makes out of them very efficient adsorbents or catalysts.

Zeolites are a versatile alternative to alumina and activated carbon for recovery of volatile organic compounds (VOCs). Hydrocarbon adsorption has been extensively studied on NaX zeolite [2,3], and more recently, on CaA molecular sieves [4,5].

Zeolites are also a suitable support for transition metals due to their open structure and ion exchange capacities [6] with many applications in heterogeneous catalysis. Transition metal (Co^{2+}, Fe^{3+}, Cu^{2+} and Cu^+) exchanged zeolites ZSM-5 have been successful tested for the oxydehydrogenation of ethane with oxygen [7] and the oxidation of propane has been carried out over Fe^{3+}, Co^{2+} and Mn^{2+} exchanged zeolite ZSM-5 [8]. SO_2 oxidation has been carried out with Mn^{2+} heterogenised on NaX zeolite [6]. Moreover, Fe^{3+}, Co^{2+} and Mn^{2+} have been found to be the most active metals in methane combustion [9,10]. Although data are available on the sorption behaviour of *n*-hexane on Co^{2+}, Ni^{2+}, Zn^{2+} and Cd^{2+} exchanged NaX zeolites [11], they are scarce for transition metal exchanged zeolites in connection with removal of pollutants [12].

The techniques of gas–solid chromatography or inverse gas chromatography (IGC) provide information on thermodynamic, surface energy, morphological parameters (such as surface area and porosity) and reaction kinetics, associated with gas–solid adsorption and catalytic reactions. IGC has

* Corresponding author. Tel.: +34 985 103437; fax: +34 985 103434.
E-mail address: sordonez@uniovi.es (S. Ordóñez).

0021-9673/$ – see front matter © 2004 Elsevier B.V. All rights reserved.
doi:10.1016/j.chroma.2004.07.065

been widely utilized in the past years to study zeolites [13], adsorbents [14] foods [15], carbon blacks [16] and fibers [17].

In the present work, transition metals (Co^{2+}, Mn^{2+} and Fe^{3+}) were incorporated into the zeolitic structures of NaX and CaA. Adsorbents surface properties such as surface area and acidity were characterized by nitrogen adsorption and ammonia-temperature programmed desorption (TPD), respectively. Adsorbents performance for the removal of several alkanes, cyclic hydrocarbons, aromatic hydrocarbons and chlorinated compounds was determined by IGC following the same procedure used in our previous works [18,19].

2. Experimental

2.1. Materials

Two adsorbents, zeolites NaX and CaA (40/60 mesh, Alltech), have been studied and compared with several metal cation-exchanged zeolites. The exchange procedure consisted of keeping the zeolite in an aqueous solution of the metal ion under stirring at 70 °C for 24 h, followed by heating in a furnace at 500 °C for 4 h.

Metal ion solutions (0.25 M) were prepared by dissolving 18.18 g of $Co(NO_3)_2{\cdot}6H_2O$ (Merck), 25.25 g of $Fe(NO_3)_3{\cdot}9H_2O$ (Panreac) and 15.68 g of $Mn(NO_3)_2{\cdot}4H_2O$ (Panreac) into a 250 cm^3 of distilled water. Ion exchange between zeolites and Co^{2+}, $Fe^{3+}$and Mn^{2+} solutions was carried out by suspending 3 g of zeolite into the metal ion solution at 70 °C with mild stirring in a water bath for 24 h. The preparation of Fe^{3+}exchanged LTA zeolites (CaA) has to be carried out at low pH, in order to avoid the precipitation of iron hydroxide [20]; the pH was adjusted by addition of H_2SO_4. The suspension was then filtered and the cake rinsed with distilled water; the solid was then heated in a furnace at 500 °C for 4 h. The unit cell chemical composition of all samples was determined by ICP-mass spectroscopy. Results are shown in Table 1.

Zeolites structures were determined by X-ray diffraction (XRD) (Philips PW1710 diffractometer) working with the Kα line of copper. The powder diffraction standards (JCPDS) were used for proper interpretation of the crystal structure. Surface area and pore volume were determined by nitrogen adsorption at −196 °C (Micromeritics ASAP 2000 surface analyser), assuming a value of 0.164 nm^2 for the cross-section of the nitrogen molecule.

Table 1
Unit cell composition of zeolites

Zeolites	Unit cell composition	Na/Ca exchanged (%)
NaX	$Na_{88}(AlO_2)_{88}(SiO_2)_{104}$	–
Co–NaX	$Na_{47}Co_{20.3}(AlO_2)_{88}(SiO_2)_{104}$	46.59
Mn–NaX	$Na_{48.57}Mn_{20}(AlO_2)_{88}(SiO_2)_{104}$	44.81
Fe–NaX	$Na_2Fe_{43}(AlO_2)_{88}(SiO_2)_{104}$	97.73
CaA	$Ca_{45.85}(AlO_2)_{96}(SiO_2)_{96}$	–
Co–CaA	$Ca_{27.91}Co_{17.94}(AlO_2)_{96}(SiO_2)_{96}$	39.13
Mn–CaA	$Ca_{3.52}Mn_{42.32}(AlO_2)_{96}(SiO_2)_{96}$	92.32
Fe–CaA	$Ca_{0.85}Fe_{45}(AlO_2)_{96}(SiO_2)_{96}$	98.15

The solutes used as supplied were: *n*-pentane, *n*-hexane, *n*-heptane and *n*-octane (Fluka >99.5% purity), and cyclohexane, cycloheptane, benzene, chloroform, trichloroethylene and tetrachloroethylene (Panreac >99% purity). Helium as carrier gas (>99.9995% purity, according to the manufacturer Air Liquide) was used as supplied.

2.2. Apparatus and procedure

A conventional gas chromatograph (Varian 3800) with a thermal conductivity detector (TCD) was used for the adsorption measurements. A loading of 0.6 g of each zeolite was placed into a 27 cm length of Supelco Premium grade 304 stainless steel column, with passivated inner walls and an inside diameter of 5.3 mm (o.d. 0.25 in.). Each column was packed with mechanical vibration, and the two ends were plugged with silane-treated glass wool. The columns were stabilized in the GC system at 250 °C overnight under a helium flow rate of 30 mL/min. In order to avoid detector contamination, the column outlet was not connected to the detector during this period.

Measurements were carried out in the temperature range of 200–270 °C. Helium was used as carrier gas, and flow rates were measured using a calibrated soap bubble flowmeter. In order to meet the requirement of adsorption at infinite dilution, corresponding to zero coverage and GC linearity [21], the samples injected were in the range from 0.05 to 0.8 μL. For each measurement, the sample was injected three times, obtaining reproducible results (0.5%). The specific retention volume, V_g, in cm^3/g, was calculated from the equation:

$$V_g = Fj\frac{t_R - t_M}{m}\left(\frac{p_0 - p_w}{p_0}\right)\left(\frac{T}{T_{meter}}\right) \quad (1)$$

where F is the carrier gas flow-rate, t_R the retention time in min, t_M the retention time of a non-adsorbing marker (air), p_0 the outlet column pressure, p_i the inlet pressure, p_w the vapour pressure of water at the flowmeter temperature, T_{meter} the ambient temperature in K, and j is the James–Martin compressibility factor.

In order to separate the surface adsorption contribution from the total retention data, the absence of mass-transfer effects must be ensured. Preliminary experiments show that in the most stringent case (cyclohexane, cycloheptane, benzene, trichloroethylene and tetrachloroethylene over X zeolites), flow rates higher than 50 mL/min leads to V_g independent from gas flow rate. So, a gas flow rate of 50 mL/min was used in the adsorption experiments carried out in this work.

Table 2
Textural properties of zeolites under investigation

Zeolites	$S_{Langmuir}$ (m^2/g)	$V_{mesopores}$ (BJH) (cm^3/g)	$V_{micropores}$ (t-Lippens) (cm^3/g)	Average pore diameter (Å)	a_0 (Å)[a]
NaX	571	0.165	0.170	22.75	25.10
Co–NaX	633	0.176	0.178	21.25	25.00
Mn–NaX	720	0.135	0.220	19.61	24.95
Fe–NaX	245	0.253	0.001	48.31	25.11
CaA	549	0.062	0.176	22.75	24.52
Co–CaA	422	0.138	0.093	42.13	24.49
Mn–CaA	553	0.071	0.167	21.64	24.40
Fe–CaA	301	0.333	0.004	50.88	24.57

[a] Calculated from the 10 most intense diffraction peaks in the range $2\theta = 30–90^\circ$.

3. Results and discussion

3.1. Textural characterization of zeolites

Zeolites surface area and pore volume, measured by N_2 physisorption, are summarized in Table 2, and pore size distribution is shown in Fig. 1. According to IUPAC recommendations for microporous materials, surface area and micropore volume were calculated using the Langmuir and Lippens "t" method [22,23]. Mesopore volumes were obtained from the analysis of the desorption branch of the nitrogen isotherm using the Barrett–Joyner–Halenda (BJH) method.

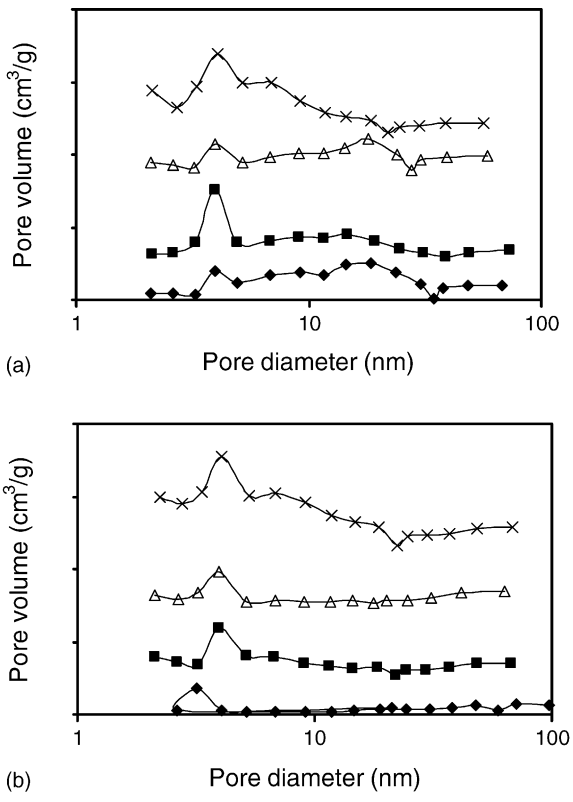

Fig. 1. Pore size distribution calculated from nitrogen adsorption isotherms by the BJH method for parent zeolite (♦), Co-zeolite (■) Mn-zeolite (△) and Fe-zeolite (X) for: (a) NaX, (b) CaA.

Textural properties were evaluated for the NaX and CaA zeolites before and after thermal treatment at 500 °C. Zeolite NaX undergoes a slight reduction of surface area and change in porous structure, whereas zeolite CaA has the opposite behaviour. Results reveal that the maximum in the pore size distribution for all the exchange zeolites is shifted to higher pore volumes. Cobalt and manganese exchanged zeolites show only small variations with respect to the original ones. However, iron exchanged zeolites show a large decrease in surface area and micropore volume, whereas its mesopore volume and average pore diameter increase. Being the treatment conditions the same in all cases, this behaviour must be due to deposition on the zeolite channels as well as outer surfaces of Fe species. This is supported by the XRD patterns that show evidence of the presence of α-Fe_2O_3 species [24]. The slight increase in the average pore diameter can be explained by two simultaneous effects: slight increase of the mesopore volume, and sharp decrease of micropore volume.

XRD profiles were obtained for the eight zeolitic samples and are shown in Fig. 2. The unit cell parameters, a_0, of the cubic patterns, determined by Bragg equation [25], are summarized in Table 2; they are similar to previous data reported in the literature [26]. The characteristic peaks for the fresh zeolites are shifted or distorted after ion exchange takes place. The unit cell volume of Fe/zeolite, NaX as well as CaA, increased markedly with respect to the NaX or CaA zeolites. These exchanged zeolites show a clear decrease in crystallinity if compared to the original NaX or CaA; the reflections attributed to the zeolite structure are less intense after the exchange of the cation. The same behaviour has been reported in the literature, comparing the reflections in the case of ion exchange and impregnation, being the last ones much more intense [27]. The decrease of peak intensity as the iron content increases, shows that iron addition has a negative effect on crystallinity, which has also been noticed in the case of zeolite HSM [28], NaY [29] and FSM and NaY [24]. Furthermore, when cobalt or manganese enter into the zeolitic structure, it maintains its identity, with an unusual slight decrease in cell volume. The low values of the lattice parameters, as compare to those of NaX and CaA, may be explained by the low amount of metal exchanged by the zeolite, as it can be concluded from ICP-mass values shown

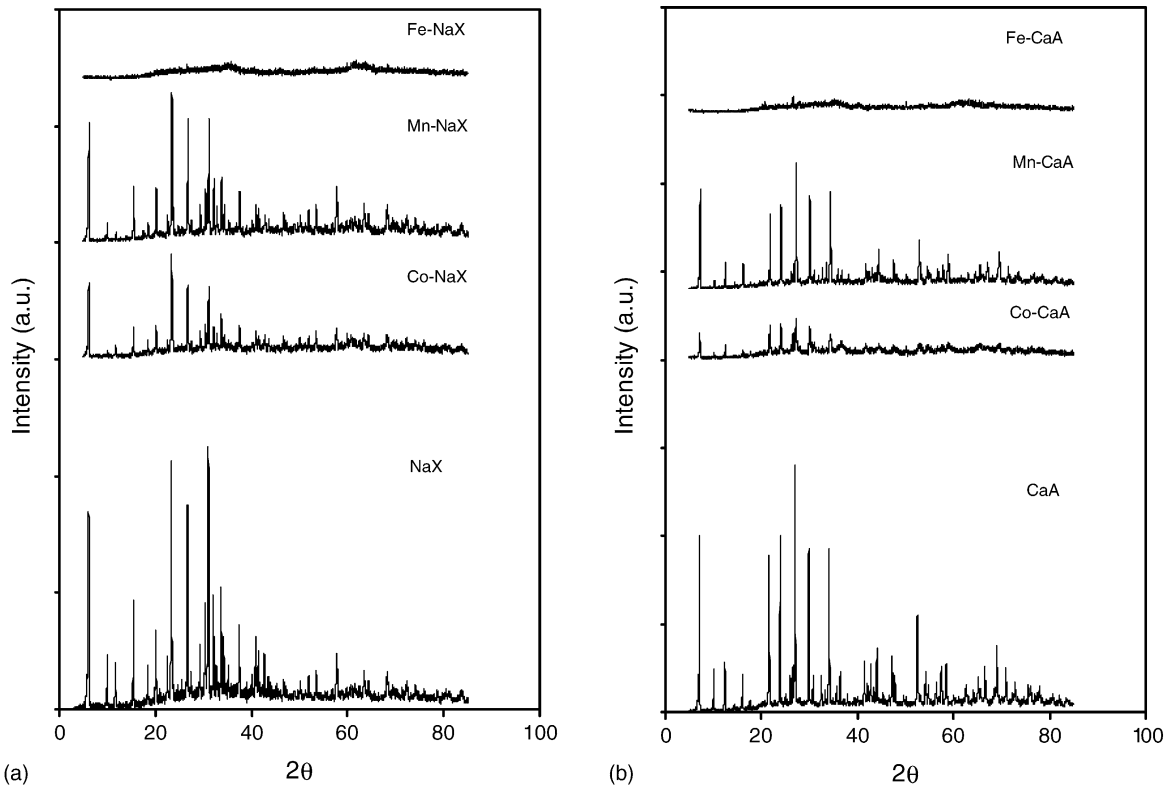

Fig. 2. XRD patterns of parent zeolites and their derivates: (a) NaX, (b) CaA.

in Table 1. None of the XRD spectra show sharp peaks for transition metal oxides, which may prove the high dispersion and/or low crystalline nature (amorphous) of the metal oxides on the zeolitic support [30]. Careful analysis of the former pattern provides evidence of the presence of a small line at $2\theta = 38^\circ$ due to α-Fe_2O_3. The estimated particle size is found to be 2 and 6 nm for Fe–NaX and Fe–CaA, respectively, as determined from Scherrer equation.

It has been pointed out that the cation size and its coordination state play an important role regarding its incorporation into the zeolitic skeleton [31]. The ionic radii, of the following ions are in the order: Si^{4+} (40 Å) < Al^{3+} (53 Å) < Fe^{3+} (69 Å) < Co^{2+} (79 Å) < Mn^{2+} (81 Å) [32]. This sequence does not agree with the amount of metal attached to the zeolitic material, which is in the order: $Co^{2+} < Mn^{2+} < Fe^{3+}$. Trivalent cations seem to have stronger affinity with exchange sites than divalent ones, and thus they show a higher degree of exchange. This behaviour has also been reported in the literature [29].

The evolution of lattice parameters with ionic radii of the exchanged metal is shown in Fig. 3. The variation of the lattice parameters of the cubic cell depends on the cation ionic radius. For both zeolites (NaX and CaA), the lattice parameter decreases with the cation ionic radius attached to the zeolitic structure, taking into account that Fe increases the unit cell parameter. Co-zeolite and Mn-zeolite decrease the structural cell, much more in the case of a Mn-dopant, which has the higher ionic radius.

3.2. Adsorption studies by IGC

3.2.1. Adsorption parameters

Adsorption parameters for hydrocarbons (C_5–C_8), cyclic compounds (cyclohexane and cycloheptane), aromatic compounds (benzene), and chlorinated ones (chloroform, trichloroethylene and tetrachloroethylene) on zeolites NaX and CaA, as well as those materials resulting from the ion exchange with transition metals, were determined in the infinite dilution region (Henry's law region). The solutes have been chosen because they are potential gas pollutants and the determination of adsorption parameters and their relationship

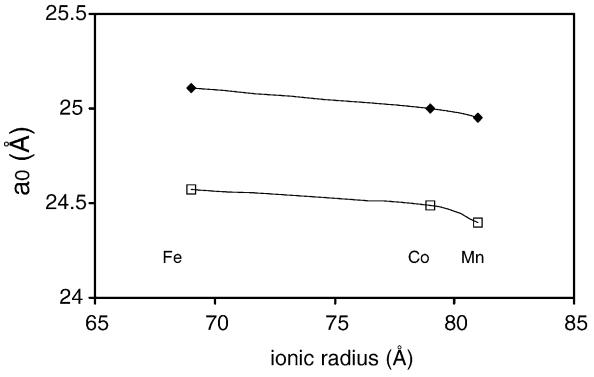

Fig. 3. Effect of metal ionic radius on the lattice parameter for zeolite NaX (♦) and zeolite CaA (□).

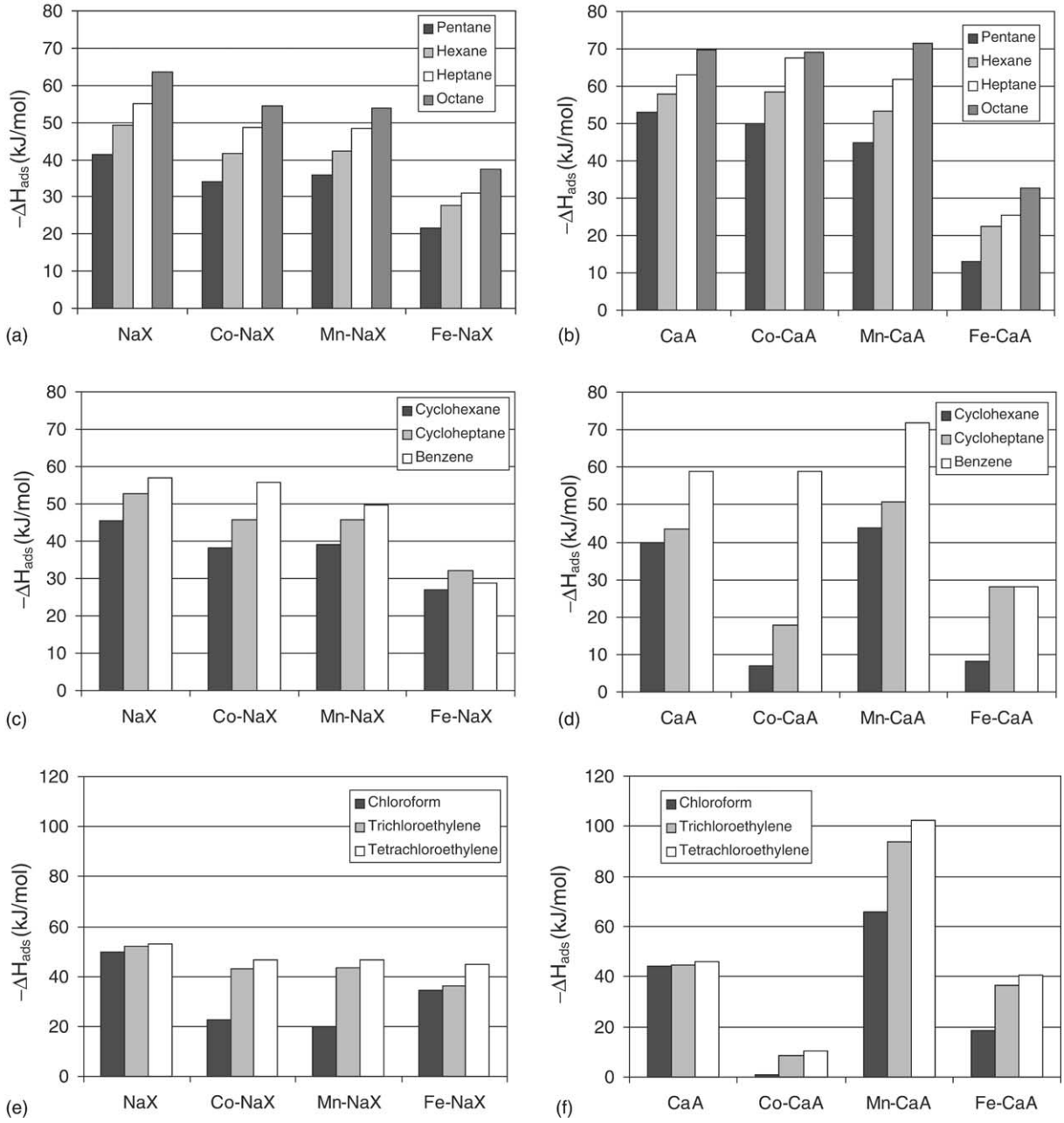

Fig. 4. Adsorption enthalpies (kJ/mol) for alkanes (a and b), cyclic and aromatic compounds (c and d), and chlorinated compounds (e and f) on different adsorbents.

with molecular interactions are important in the selection of adsorbents for their removal.

Fig. 4 shows the values of adsorption enthalpies for the *n*-alkanes and other molecules over the various zeolites. These values were estimated using Eq. (2) and plots of $\ln V_g$ versus $1/T$.

$$\Delta H_{ads} = -R\frac{\partial(\ln V_g)}{\partial(1/T)} \quad (2)$$

For all adsorbents the adsorption enthalpy of *n*-alkanes increases with the carbon number. Benzene exhibits a more negative ΔH_{ads} than cyclic hydrocarbons and aliphatic and alicyclic hydrocarbons with the same carbon number, i.e. hexane and cyclohexane. Similar results were found by Bilgiç and Aşkin [5] for zeolite CaA and İnel et al. [3] for zeolite NaX. For chlorinated compounds the adsorption enthalpy increases with molecular size, in the sequence: chloroform < trichloroethylene < tetrachloroethylene.

It is noteworthy that the adsorption enthalpies are higher in the case of zeolites NaX or CaA without any modification, than in the other cases, with the exception of Co–CaA and Mn–CaA, for certain adsorbates. In the case of zeolite NaX and derivates, NaX gives the highest adsorption enthalpies, followed by Mn–NaX and Co–NaX. Different behaviour is

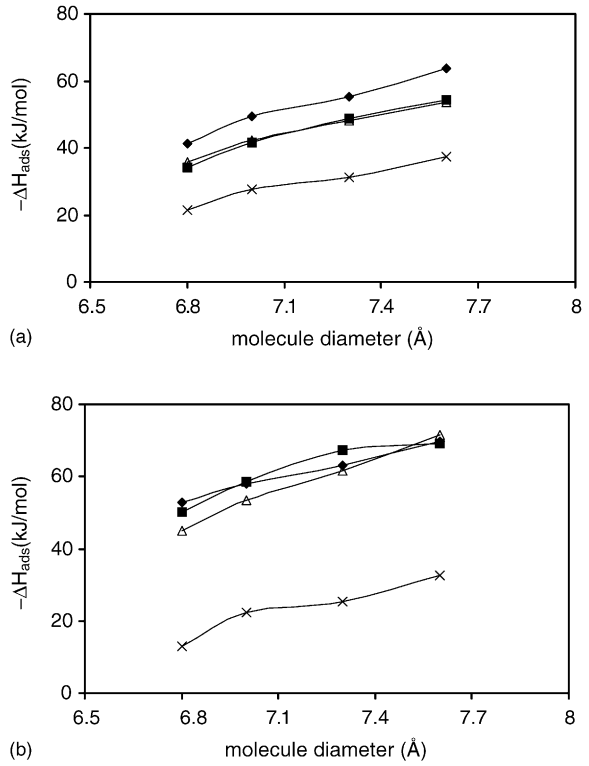

Fig. 5. Adsorption enthalpies of zeolites vs. molecular diameter of alkanes for parent zeolite (♦), Co-zeolite (■), Mn-zeolite (△) and Fe-zeolite (X) for: (a) NaX, (b) CaA.

observed for zeolite CaA and derivates; in this case CaA gives a higher adsorption enthalpy for *n*-alkanes, and the zeolite Mn–CaA exhibits the largest interactions with the cyclic, aromatic and chlorinated compounds, presumably because of its high percentage of Mn^{2+}. Although both type of zeolites, NaX and CaA, with FAU and LTA structures, respectively, are hydrophilic zeolites [6], they allow a better diffusion of cations in solution, and Mn^{2+} ion exchange loading is higher in the case of zeolite CaA than in the case of zeolite NaX. This behaviour has been reported in the literature for the same cation [6]. Furthermore, zeolite Co–CaA exhibits a selective behaviour for aromatic compounds, whereas its adsorption enthalpy for chlorinated compounds is very low.

The evolution of adsorption enthalpy with the molecule diameter (calculated from the cross-section area of the molecule, considered spherical) is depicted in Fig. 5. This figure illustrates how adsorption enthalpies, obtained by IGC, can contribute to the fundamental understanding of zeolitic molecular sieves and their derivates. Results suggest that zeolites interactions are not a function, in this case, of their pore diameter, because they are larger than the solute diameter. Similar representations for enthalpies of immersion of zeolites into different liquids, as function of their molecular size, have been obtained to evaluate the accessibility to the microporous network [33]. However, the lowest adsorption values correspond to the lowest surface area and micropore volume (Fe-exchanged zeolites). A linear trend is observed for the *n*-alkanes, which also holds for chlorinated or cyclic compounds.

From chromatographic data the standard free energy of adsorption at infinite dilution, ΔG_{ads} (J/mol), is given by [5,34,35]:

$$\Delta G_{ads} = -RT \ln \left[\frac{p_0 V_g}{\pi_0 A} \right] \quad (3)$$

or in an equivalent form [34,36]

$$\Delta G_{ads} = -RT \ln V_g + C \quad (4)$$

where A is the specific surface area, and π_0 is the spreading pressure of the adsorbed gas in the De Boer standard state, which was taken as 338 μN/m [37]. Parameter C is a constant related to the standard states. Data of ΔG_{ads} for the solute–sorbent systems calculated from Eq. (3), at 250 °C, are given in Fig. 6. The free energy of adsorption for *n*-alkanes increases with the carbon number and follows the same trend as the adsorption enthalpies.

For a given adsorbate, the free energy of adsorption is the sum of the energies of adsorption attributed to dispersive and specific interactions. The standard free energy of adsorption takes into account the standard free energy of adsorption of polar solutes on solid surfaces, namely, the dispersive contribution, ΔG^{d}_{ads}, and the specific contribution, ΔG^{s}_{ads} [38].

As in the case of the free energy of adsorption, the surface free energy of the adsorbent, γ_S (J/m^2), may be split into dispersion, γ^D_S, and specific, γ^S_S, contributions, corresponding to the dispersion and specific interactions, respectively:

$$\gamma_S = \gamma^S_S + \gamma^D_S \quad (5)$$

The interaction between the stationary phase and the adsorbate can be attributed to polar or non-polar (dispersive) van der Waals forces. The interaction between *n*-alkanes, with non-preferential localization of electrons, and the stationary phase involves only dispersive forces. The dispersive component, intrinsic and unspecific for all molecules, is given according to Dorris and Gray [39] by:

$$\gamma^D_S = \frac{1}{4} \frac{\Delta G^2_{CH_2}}{\gamma_{CH_2} N^2 a^2_{CH_2}} \quad (6)$$

where N is the Avogadro number, a_{CH_2} is the area occupied by a –CH_2 group (0.06 nm^2), and γ_{CH_2} (mJ/m^2) is the surface tension of a surface consisting of CH_2 groups, which is a function of temperature in °C:

$$\gamma_{CH_2} = 35.6 + 0.058(20 - T) \quad (7)$$

For *n*-alkanes $\Delta G_{ads} = \Delta G^{d}_{ads}$ and it changes with the number of carbon atoms in the molecules; the incremental adsorption energy corresponding to a methylene group, ΔG_{CH_2}, may be calculated from [40]:

$$\Delta G_{CH_2} = -RT \ln \frac{V_{g(n)}}{V_{g(n+1)}} \quad (8)$$

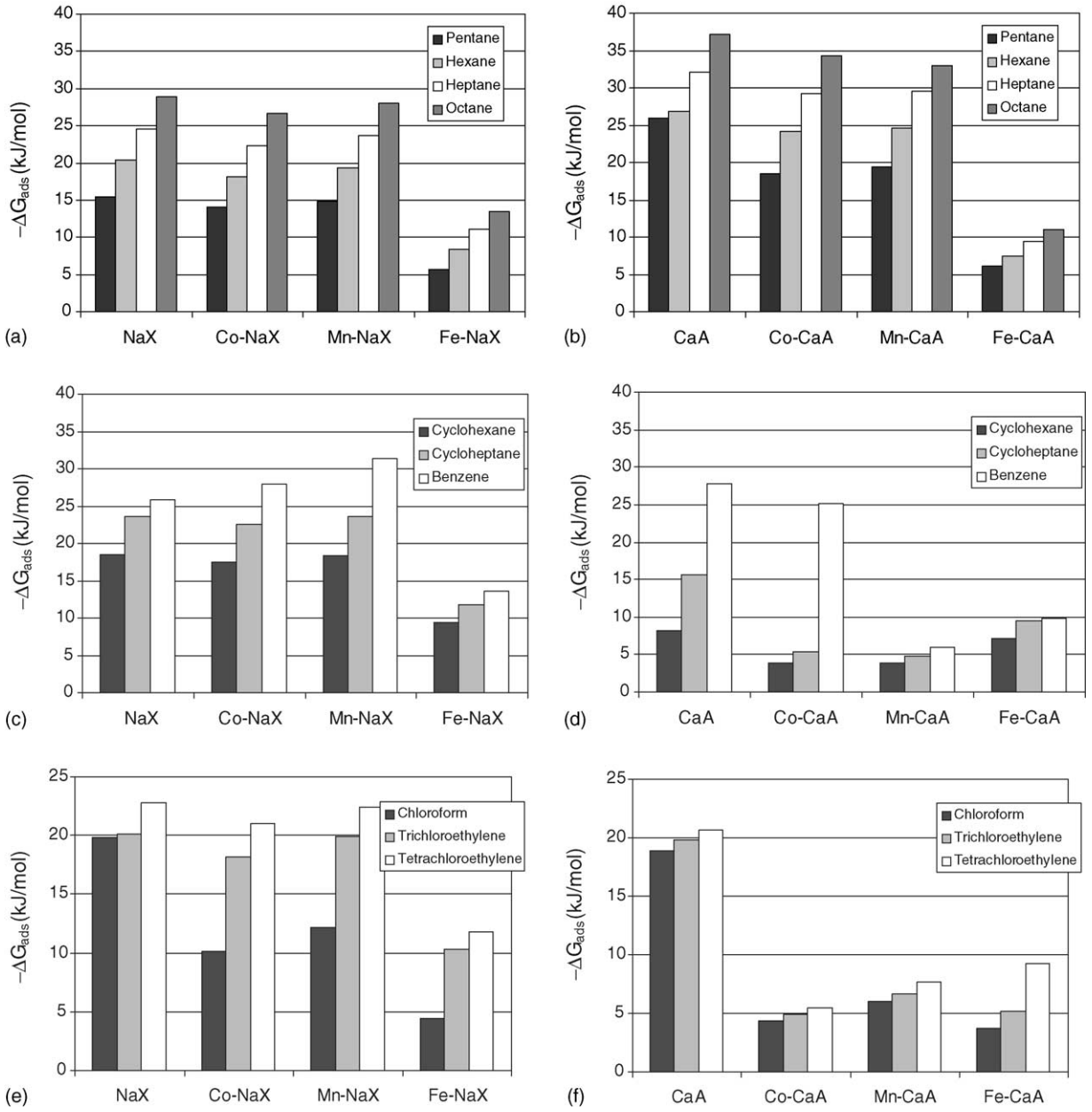

Fig. 6. Standard free energy, ΔG_{ads} (kJ/mol), for alkanes (a and b), cyclic and aromatic compounds (c and d), and chlorinated compounds (e and f) on adsorbents under study at 250 °C.

where $V_{g,n}$ and $V_{g,n+1}$ are the specific retention volumes of two consecutive *n*-alkanes having *n* and (*n*+1) carbon atoms, respectively. ΔG_{CH_2} is independent of the chosen reference state of adsorbed molecule [34]. The slopes of linear functions represent the increment in ΔG_{CH_2}.

Calculated γ_S^D values from Eq. (6) are shown in Table 3; they decrease as temperature increases in all cases. The evolution of γ_S^D with column temperature for the different samples is shown in Table 3. Values of γ_S^D for all zeolites excepting Fe exchanged, are much higher than those obtained for polymers, ~60 mJ/m^2 [35] or compounds such as theophylline and caffeine, ~50 mJ/m^2 [41]. The high γ_S^D values are presumably associated to a high interaction potential in the micropores, as an increase of microporous volume corresponds to an increase of the dispersive component of the surface energy. Furthermore, those samples which show less crystalinity have lower values of the dispersive component of surface energy, whereas the original zeolites and the Co^{2+} and Mn^{2+} exhanged ones have the highest values. Briefly stated, the higher the dispersive component, the lower is the slope of γ_S^D versus column temperature.

In order to get a better understanding of the role of specific adsorption mechanisms, the chromatographic behaviour of polar molecules was compared to that of *n*-alkanes.

The specific component of the surface free energy is closely related to the parameter of specific interaction of polar

Table 3
Dispersive component of surface free energy, γ_S^D (mJ/m^2) and the slope of γ_S^D vs. column temperature

	200 °C	230 °C	250 °C	270 °C	Slope
NaX	154.9	153.1	152.3	150.3	−0.0629
Co–NaX	150.8	146.6	144.3	145.2	−0.0864
Mn–NaX	169.3	164.0	162.6	155.8	−0.1809
Fe–NaX	56.8	54.4	43.3	26.8	−0.4202
CaA	242.0	241.1	232.6	226.9	−0.2255
Co–CaA	229.0	230.3	224.5	209.5	−0.2607
Mn–CaA	204.5	200.5	197.3	195.4	−0.1342
Fe–CaA	28.7	24.0	19.8	13.7	−0.2115

solutes (I^{sp}). This parameter involves the surface properties in terms of potential and acid–base interactions, as for instance, Keesom, Debye and hydrogen bonding, and can be determined from the free energy of adsorption increment, $\Delta(\Delta G)$, between a polar solute and the real or hypothetical *n*-alkane that have the same cross-section surface area (it is supposed to present negligible specific component of the interaction) [35].

$$I^{sp} = \frac{\Delta(\Delta G)}{N a_p} \tag{9}$$

where a_p is the cross-section area of the probe molecule. In the present work, a_p is calculated from the liquid density, ρ and the molar weight of the molecule, M assuming a spherical molecular shape in a hexagonal close-packed configuration [42].

$$a_p = 1.09 \times 10^{14} \left(\frac{M}{\rho N} \right)^{2/3} \tag{10}$$

The specific interaction parameters, I^{sp} calculated from Eq. (9), for the zeolites studied, are listed in Table 4. Results indicate how difficult is to obtain accurately the dispersive component of the interaction energy. The specific interaction parameter decreases as the temperature increases. However, it does not vary consistently with molecular area of solute, which means that the pore diameter is not the key factor in polar interactions, as it was shown in a previous work [19]. Within a certain family, the interaction for cyclic hydrocarbons does not vary uniformly, cycloheptane and cyclohexane show similar values, but the largest interaction value depends on the adsorbent. Furthermore, I^{sp} is higher for the aromatic ring (benzene) than for cycloalkanes. When benzene adsorbs on zeolites, there are two kinds of adsorption sites, i.e. Lewis acid sites, which is represented by the cation site interacting with the benzene ring, and the Lewis base sites, namely, oxygen atoms in the zeolite structure, that have a very high interaction with benzene. In fact, benzene interacts strongly with all the zeolites with the only exception of Co–CaA and Mn–CaA. For Mn–NaX and Co–NaX, the specific interaction is very strong. Co–CaA shows the same behaviour, again Mn–CaA being different and hence adsorption on cations takes place predominantly in Mn-zeolites.

Table 4
I^{sp} (mJ/m^2) values determined for zeolites under study

Solutes	200 °C	230 °C	250 °C	270 °C
Zeolite NaX				
Cyclohexane	19.1 ± 2.3	18.1 ± 1.9	15.5 ± 1.3	13.8 ± 2.5
Cycloheptane	25.7 ± 2.6	24.7 ± 4.9	23.1 ± 2.1	21.3 ± 2.7
Benzene	96.2 ± 4.8	93.1 ± 5.8	88.8 ± 4.2	84.2 ± 3.7
Chloroform	24.6 ± 2.1	20.3 ± 3.0	11.1 ± 1.0	5.2 ± 0.6
Trichloroethylene	66.6 ± 3.2	63.8 ± 4.1	61.2 ± 2.3	55.4 ± 3.4
Tetrachloroethylene	51.6 ± 4.0	47.7 ± 2.8	45.7 ± 3.1	43.3 ± 2.5
Zeolite Co–NaX				
Cyclohexane	24.7 ± 3.4	24.2 ± 4.0	23.7 ± 3.5	24.2 ± 3.6
Cycloheptane	30.7 ± 4.5	30.6 ± 4.9	30.1 ± 5.0	29.9 ± 4.3
Benzene	120.1 ± 6.4	117.2 ± 7.9	116.5 ± 6.8	110.1 ± 8.3
Chloroform	2.2 ± 0.4	1.7 ± 0.4	1.5 ± 0.6	1.4 ± 0.3
Trichloroethylene	67.8 ± 4.3	64.3 ± 3.8	63.1 ± 3.8	61.3 ± 3.6
Tetrachloroethylene	55.7 ± 5.3	53.2 ± 6.0	52.4 ± 5.5	50.7 ± 5.9
Zeolite Mn–NaX				
Cyclohexane	24.7 ± 4.3	24.3 ± 3.8	23.9 ± 4.9	23.6 ± 4.5
Cycloheptane	30.7 ± 5.0	30.3 ± 4.2	30.2 ± 4.2	29.7 ± 4.0
Benzene	134.6 ± 8.9	132.2 ± 10.0	126.5 ± 7.8	120.8 ± 9.3
Chloroform	0.8 ± 0.2	0.7 ± 0.1	0.5 ± 0.3	0.4 ± 0.05
Trichloroethylene	72.3 ± 6.4	70.5 ± 6.8	69.1 ± 5.9	68.9 ± 7.2
Tetrachloroethylene	57.6 ± 4.8	56.1 ± 4.8	55.7 ± 5.0	54.6 ± 4.2
Zeolite Fe–NaX				
Cyclohexane	24.7 ± 4.6	22.0 ± 3.8	14.7 ± 3.9	10.0 ± 4.1
Cycloheptane	22.5 ± 5.1	19.0 ± 3.7	16.4 ± 4.1	12.2 ± 3.5
Benzene	67.9 ± 5.3	60.2 ± 5.6	46.8 ± 5.7	34.0 ± 4.3
Chloroform	31.0 ± 4.3	28.2 ± 5.0	12.0 ± 4.1	9.0 ± 3.5
Trichloroethylene	49.8 ± 4.6	44.8 ± 3.6	37.1 ± 4.1	29.6 ± 3.0
Tetrachloroethylene	41.2 ± 3.5	40.6 ± 4.1	30.9 ± 5.0	23.2 ± 3.5
Zeolite CaA				
Cyclohexane	89.0 ± 6.2	67.3 ± 5.9	58.1 ± 4.8	52.6 ± 5.1
Cycloheptane	107.5 ± 6.3	91.2 ± 7.3	79.9 ± 6.0	37.6 ± 5.7
Benzene	135.1 ± 8.3	91.6 ± 7.4	76.3 ± 7.0	52.8 ± 5.3
Chloroform	20.7 ± 2.5	22.3 ± 3.2	15.9 ± 1.9	1.1 ± 0.1
Trichloroethylene	67.5 ± 3.2	54.9 ± 4.2	46.9 ± 3.8	27.2 ± 2.7
Tetrachloroethylene	65.3 ± 4.1	62.7 ± 3.2	44.9 ± 2.0	17.6 ± 1.9
Zeolite Co–CaA				
Cyclohexane	82.0 ± 3.9	74.4 ± 4.0	59.6 ± 1.9	51.2 ± 2.4
Cycloheptane	63.2 ± 3.2	51.1 ± 2.8	37.0 ± 1.5	29.3 ± 1.4
Benzene	133.2 ± 5.0	125.5 ± 4.3	109.0 ± 2.9	99.3 ± 3.0
Chloroform	99.9 ± 3.4	90.0 ± 3.2	74.7 ± 3.5	65.9 ± 2.4
Trichloroethylene	156.8 ± 5.9	152.0 ± 5.2	134.8 ± 3.6	124.3 ± 4.2
Tetrachloroethylene	142.6 ± 4.8	124.5 ± 3.8	108.2 ± 4.0	98.4 ± 3.5
Zeolite Mn–CaA				
Cyclohexane	4.8 ± 1.3	4.7 ± 0.5	4.5 ± 0.8	4.3 ± 0.4
Cycloheptane	4.7 ± 1.2	4.5 ± 1.4	4.2 ± 0.3	4.2 ± 0.5
Benzene	6.8 ± 1.8	6.8 ± 1.7	6.4 ± 1.4	6.2 ± 0.7
Chloroform	4.9 ± 0.8	4.6 ± 0.3	4.0 ± 0.8	3.6 ± 0.5
Trichloroethylene	9.5 ± 1.7	9.4 ± 1.9	9.2 ± 1.3	9.0 ± 0.5
Tetrachloroethylene	7.7 ± 1.4	7.1 ± 0.4	7.0 ± 1.2	6.7 ± 1.4
Zeolite Fe–CaA				
Cyclohexane	9.13 ± 1.5	7.8 ± 1.8	6.7 ± 1.8	5.9 ± 1.3
Cycloheptane	15.8 ± 1.4	12.4 ± 1.7	12.0 ± 1.5	10.6 ± 0.5
Benzene	44.7 ± 2.3	37.8 ± 1.9	36.5 ± 2.0	26.8 ± 1.9
Chloroform	21.8 ± 1.8	14.2 ± 1.2	9.2 ± 0.4	9.1 ± 0.5
Trichloroethylene	32.6 ± 1.9	16.7 ± 1.7	11.7 ± 0.7	10.6 ± 0.8
Tetrachloroethylene	27.8 ± 1.8	23.8 ± 2.0	21.5 ± 0.7	19.5 ± 1.8

Specific interactions between chlorinated adsorbates and zeolites depend on size, dipolar moment and polarity of the molecule. Their specific interaction parameters follow the expected trend on the basis of their dipolar moment trichloroethylene (1.78 debyes), tetrachloroethylene (1.32 debyes) chloroform (1.01 debyes) [43], i.e. stronger interactions as polarity increases, with the exception of protoned zeolites, where the interaction order is: chloroform > trichloroethylene > tetrachloroethylene. It is noteworthy that zeolite Co–CaA exhibits a very high trichloroethylene interaction, very similar to that of chloroform and benzene.

4. Conclusions

Inverse gas chromatography has been used to study the adsorption of *n*-alkanes and other polar probes on zeolites NaX, CaA and their derivates: Co, Mn and Fe exchanged ones. Zeolites characterization was carried out by XRD and ICP-MS. Properties such as enthalpy of adsorption, free energy of adsorption and surface free energy, as well as the dispersive and specific component, are reported. Furthermore, surface acidity was studied by ammonia-TPD analysis. The following conclusions were reached:

1. Adsorption enthalpies have small variations when the cation is exchanged, just slight decreases were observed.
2. The dispersive component of the surface energy increases with the micropore volume, and a relationship exists between the dispersive component and the slope of the straight line which represent the evolution of the dispersive component of surface energy as function of column temperature.
3. Adsorption properties depend on what cation is exchanged. Interactions between benzene and the adsorbent are much stronger in the case of zeolites Mn–NaX and Co–NaX, whereas for chlorinated compounds and zeolites interactions are stronger for zeolite Co–CaA. The trivalent cation (Fe^{3+}) does not seem to increase neither the adsorption efficiency, nor the specific interaction.

Acknowledgements

Financial support from the Asturias Regional Research program, project PR-01-GE-17, is gratefully acknowledged. One of the authors (E.D.) acknowledges the grant received from the Asturias Research Foundation (FICYT).

References

[1] D.W. Breck, Zeolite Molecular Sieves, John Wiley, New York, 1974.
[2] P.D. Hopkins, J. Catal. 29 (1973) 112.
[3] O. İnel, D. Topaloğlu, A. Aşkin, F. Tümsek, Chem. Eng. J. 88 (2002) 255.
[4] F. Tümsek, O. Inel, Chem. Eng. J. 94 (2003) 57.
[5] C. Bilgiç, A. Aşkin, J. Chromatogr. A 1005 (2003) 281.
[6] J. García-Martínez, D. Cazorla-Amorós, A. Linares-Solano, Appl. Catal. B 47 (2004) 203.
[7] Y.-F. Chang, G.A. Somorjai, H. Heinemann, J. Catal. 154 (1995) 24.
[8] K. Nowinska, A. Waclaw, A. Izbinska, Appl. Catal. A 243 (2003) 225.
[9] L. Lisi, G. Bagnasco, P. Ciambelli, S. De Rossi, P. Porta, G. Russo, M. Turco, J. Solid State Chem. 146 (1999) 173.
[10] R. Spinicci, A. Tofanari, M. Faticanti, I. Pettiti, P. Porta, J. Mol. Catal. A 176 (2001) 247.
[11] R.V. Hercigonja, V.M. Radak, Thermochim. Acta 207 (1992) 15.
[12] F. Zaera, J. Phys. Chem. B 106 (2002) 4043.
[13] J. Xie, M. Bousmina, G. Xu, S. Kaliaguine, J. Mol. Catal. 135 (1998) 187.
[14] M.P. Elizalde-González, R. Ruíz-Palma, J. Chromatogr. A 845 (1999) 373.
[15] A. Boutboul, F. Lenfant, P. Giampaoli, A. Feigenbaum, V. Ducret, J. Chromatogr. A 969 (2002) 9.
[16] E. Papirer, E. Brendle, F. Ozil, H. Balard, Carbon 37 (1999) 1265.
[17] A. Vega, F.V. Díez, P. Hurtado, J. Coca, J. Chromatogr. A 962 (2002) 153.
[18] E. Díaz, S. Ordóñez, A. Vega, J. Coca, Microporous Mesoporous Mater. 70 (2004) 109.
[19] E. Díaz, S. Ordóñez, A. Vega, J. Coca, J. Chromatogr. A 1049 (2004) 139.
[20] P. Fejes, I. Kiricsi, K. Lázár, I. Marsi, A. Rockenbauer, L. Korecz, Appl. Catal. A 242 (2003) 63.
[21] B. Charmas, R. Leboda, J. Chromatogr. A 886 (2000) 133.
[22] K.S.W. Sing, D.H. Everett, R.A.W. Haul, L. Moscou, R.A. Pierotti, J. Rouquerol, T. Siemieniewska, Pure Appl. Chem. 57 (1985) 603.
[23] S.J. Greg, H.S. Sing, Adsorption, Surface Area and Porosity, Academic Press, New York, 1982.
[24] M.M. Mohamed, N.A. Eissa, Mater. Res. Bull. 38 (2003) 1993.
[25] H.P. Klug, L.E. Alexander, X-Ray Diffraction Procedures, 2nd ed., John Wiley & Sons, New York, USA, 1974.
[26] E.N. Coker, D.P. Roelofsen, R.M. Barrer, J.C. Jansen, H.v. Bekkum, Microporous Mesoporous Mater. 22 (1998) 261.
[27] B. Imre, I. Hannus, Z. Konya, I. Kiricsi, J. Mol. Struct. 651 (2003) 191.
[28] K. Bachari, J.M.M. Millet, B. Benaïchouba, O. Cherifi, F. Figueras, J. Catal. 221 (2004) 55.
[29] Z. Sarbak, M. Lewandowski, Appl. Catal. A 208 (2001) 317.
[30] D.A. Peña, B.S. Uphade, P.G. Smirniotis, J. Catal. 221 (2004) 421.
[31] M. Ziolek, I. Nowak, B. Kilos, I. Sobczak, P. Decyk, M. Trejda, J.C. Volta, J. Phys. Chem. Solids 65 (2004) 571.
[32] R.D. Shanon, Acta Cryst. A 32 (1976) 751.
[33] J. Silvestre-Albero, C. Gómez de Salazar, A. Sepúlveda-Escribano, F. Rodríguez-Reinoso, Colloids Surf. 187–188 (2001) 151.
[34] S.K. Milonjic, Colloids Surf. 149 (1999) 461.
[35] J. Xie, Q. Zhang, K.T. Chuang, J. Catal. 191 (2000) 86.
[36] T.J. Bandosz, K. Putyera, J. Jagiello, J.A. Schwarz, Micropor. Mater. 1 (1993) 73.
[37] J.H. De Boer, The Dynamical Character of Adsorption, Clarendon, Oxford, 1953.
[38] M.A. Montes-Morán, A. Martínez-Alonso, J.M.D. Tascón, Fuel Process. Technol. 77 (2002) 359.
[39] G.M. Dorris, D.G. Gray, J. Colloid Interface Sci. 77 (1980) 353.
[40] C. Herry, M. Baudu, D. Raveau, Carbon 39 (2001) 879.
[41] J.W. Dove, G. Buckton, C. Doherty, Int. J. Pharm. 138 (1996) 199.
[42] A. Van Asten, N. Van Veenendaal, S. Koster, J. Chromatogr. A 888 (2000) 175.
[43] R.C. Weast, Handbook of Chemistry and Physics, 69th ed., CRC Press, USA, 1988.